Effect of Connected Pipe Test Conditions on Scramjet Combustor Performance

Gnanasekar, S.[a], Ashok V.[b], Dipankar Das[b], Lazar T. Chitilappilly[a]
[a]Air Breathing Propulsion Project, Vikram Sarabhai Space Centre, Thiruvananthapuram, INDIA
[b]AeroDynamics and AeroThermal Group, Vikram Sarabhai Space Centre, Thiruvananthapuram, INDIA

Abstract
Scramjet engine combustion chamber is normally ground tested in connected pipe mode and has limitations in simulating all combustor entry parameters as in flight engine. Effect of variation in combustor entry pressure, test gas medium due to vitiation and combustor entry flow profile on combustor performance has been brought out through CFD simulations. Computations are carried out using in-house CFD software "PARAS-3D", which solves the Reynolds Averaged Navier-Stokes equations and uses 7 species 7 reaction model for combustion. Entry pressure is having substantial influence on combustor performance at pressures lower than a certain value and this pressure limit reduces for higher fuel equivalence ratios. In the case of vitiated medium, presence of CO_2 and the excess H_2O result in lower total temperatures leading to reduced pressures in the combustion chamber. Non-uniform flow profile at combustor entry is also found to lower the scramjet combustor performance due to reduced mixing.

1. INTRODUCTION
Current focus in space research is on low cost access to space and to increase reliability of space vehicles. This calls for two advanced technologies namely reusable launch vehicles and air breathing propulsion. Conventional launch vehicles use propellants consisting of fuel & oxidizer and oxidizer constitutes about 70% of it. Also, major part (about 75%) of the propellant is consumed within the atmospheric flight. Air breathing propulsion is an effective alternative in which oxidizer is used from atmosphere saving considerable weight of the launch vehicle. For various flight Mach number regimes, different air breathing cycles are used namely air breathing rocket/turbojet for low speed, ramjet for high supersonic and scramjet for hypersonic. Dual Mode Ram Jet (DMRJ) combines ramjet & scramjet operation in a single system. Scramjet with its supersonic combustion is identified as the most critical amongst the propulsion cycles which has caught attention worldwide. Critical in the design of the scramjet engine is an understanding of the complex flow field present in different regions of the system over a range of operating conditions.

Major portion of hypersonic air breathing propulsion development work is performed using ground test facilities. Two different strategies are followed for supersonic combustor testing namely i) free-jet testing and ii) connected pipe mode testing. In free-jet testing, the facility nozzle expands the flow to conditions expected at the inlet to the engine, and the flow discharged from the nozzle forms a free jet into which a complete engine model is placed. In connected pipe mode testing, the facility nozzle expands the working medium to conditions expected at the entry to the combustion chamber of the engine and the flow discharged from the nozzle enters the combustor model directly. In this type of testing, the engine inlet and nozzle are absent and hence their influence, especially that of air intake, is lacking.

A computational study is carried out to bring out the effect of variations in the flow conditions at the entry to the combustor in the connected pipe mode test with respect to that in the flight.

2. COMBUSTOR TESTING IN CONNECTED PIPE MODE & LIMITATIONS
To simulate hypersonic flight conditions in ground tests, stored high-pressure air must be heated significantly before it is expanded through a facility nozzle. Total pressure and stagnation temperature of

the gases would correspond to that in the flight. Generation of high enthalpy flows (heating) may be achieved by various techniques namely 1) shock tube heating, 2) storage heating, 3) arc heating, 4) electric heating and 5) combustion heating. There are advantages and disadvantages to each type of heating. Shock tubes provide the highest enthalpy, but have test times of the order of milliseconds. Storage heaters, such as pebble beds can provide time-dependent total conditions but may contaminate the test gas with particulates. Arc heaters can provide long test durations, but produce oxides of nitrogen. Electric heating produces a clean test gas, but power requirements are prohibitive. Heating through burning of fuel involves relatively lower cost but resultant air is vitiated. These combustion heated (or vitiated) facilities burn either hydrogen or hydrocarbons and results in the presence of species/concentrations in the test medium that are different from atmospheric air.

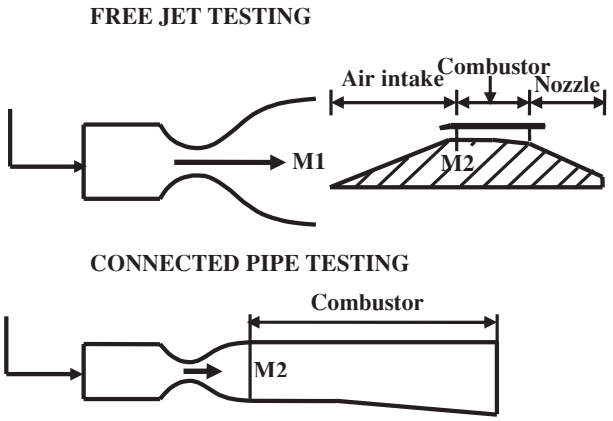

Figure 1. Scramjet combustor testing schemes

In the free-jet facility (Figure 1) the scramjet engine (consisting of hypersonic air intake, supersonic combustor and nozzle) is put into the test section and entry conditions to the air intake is simulated whereas in the connected pipe test only supersonic combustor is tested. In connected pipe test, in addition to geometry and fuel-air equivalence ratio, total temperature and Mach number are the most important parameters and are always simulated. Depending on the facility limitations, the pressure (and flow rate) would be different. Unlike in the flight, connected pipe test provides uniform flow profile at the combustor entry. In addition, when vitiated air heater is made use of, gas composition will be different. Effect of vitiation is widely studied and reported[1].

Combustion heating with oxygen replenishment to make up its composition to be same as that of atmosphere is the most popular scheme used for ground testing. After replenishment of oxygen, the incoming "air" has part of its original nitrogen replaced with combustion products. For example, Mach 10 simulation using a hydrogen combustion heater results in approximately 20% water by mole with minor concentrations of OH, H, O[2]. Hydrocarbon combustion heaters additionally result in the presence of carbon dioxide and carbon monoxide, among other species. All these vitiation species affect the thermodynamic properties of the test medium and can also affect the operation and performance of the air-breathing engine. Testing in vitiated medium is reported to result in higher ignition performance in scramjet engine[3]. The presence of combustion vitiates can affect the chemical kinetics and mode transition in a dual-mode ramjet (DMRJ)[4].

3. COMPUTATIONAL TOOL

Computations are carried out using in-house CFD software "PARAS-3D" ([5]), which solves the Reynolds averaged NS equations in flow domain inside and outside a generic geometry. PARAS-3D uses a finite volume spatial discretisation together with an explicit local time stepping scheme on a stretched rectangular mesh. The mesh is refined and unrefined using a solution adaptive technique. The numerical scheme is a TVD type, which ensures second order accuracy that reduces the numerical oscillation behind the shock discontinuity. In this time marching procedure the steady state solutions are constructed by determining time step separately for every cell from the CFL condition. The shock waves, contact discontinuities, boundary layer and body singularity like sharp edges are resolved by mesh refinement in their vicinity and mesh unrefinement in domains. Where the flow is close enough

to uniform flow. K-E model is used for computing turbulence and modified wall function is used to capture the effects of wall boundary layers .

Combustion model uses 7 species 7 reaction model of ONERA. No coupling is assumed between the turbulence and chemical kinetics, which means the reaction rates are calculated for mean temperature and mean species concentrations. The solution procedure is given below.

3.1. Governing Equations

The Navier-stokes equation is written in a conservative form using cartesian cordinates as,

$$\frac{\partial U}{\partial t} + \frac{\partial F(U)}{\partial x} + \frac{\partial G(U)}{\partial y} + \frac{\partial H(U)}{\partial z} = S \tag{1}$$

$$U = (\rho,\ \rho u,\ \rho v,\ \rho w,\ e, \rho K,\ \rho \epsilon,\ \rho_{H2},\ \rho_{O2},\ \rho_{H2O},\ \rho_{OH},\ \rho_H,\ \rho_O,\ \rho_{N2},\ \rho_{CO2})^T \tag{2}$$

is a vector of conserved variables and

$$S = (0,\ 0,\ 0,\ 0,\ 0,\ w_K,\ w_\epsilon,\ w_{H2},\ w_{O2},\ w_{H20},\ w_{OH},\ w_H,\ w_O,\ 0,\ 0)^T \tag{3}$$

is a vector of rate of production terms per unit volume.

The flux vectors **F, G** and **H** are defined as

$$\mathbf{F} = \begin{pmatrix} \rho u \\ \rho u^2 + p - \tau_{xx} \\ \rho uv - \tau_{xy} \\ \rho uw - \tau_{xz} \\ u(p + e - \tau_{xx}) - \tau_{xy} v - \tau_{xz} w + q_x + \\ \Sigma_k(\rho_k h_k u diff_k) \\ \rho ku - \frac{\mu_t}{\sigma_k}\frac{\partial K}{\partial x} \\ \rho \epsilon u - \frac{\mu_t}{\sigma_\epsilon}\frac{\partial \epsilon}{\partial x} \\ \rho_{H2}(u + udiff_{H2}) \\ \rho_{O2}(u + udiff_{O2}) \\ \rho_{H20}(u + udiff_{H20}) \\ \rho_{OH}(u + udiff_{OH}) \\ \rho_H(u + udiff_H) \\ \rho_O(u + udiff_O) \\ \rho_{N2}(u + udiff_{N2}) \\ \rho_{CO2}(u + udiff_{CO2}) \end{pmatrix} \tag{4}$$

$$\mathbf{G} = \begin{pmatrix} \rho v \\ \rho uv - \tau_{xy} \\ \rho v^2 + p - \tau_{yy} \\ \rho vw - \tau_{yz} \\ v(p + e - \tau_{yy}) - \tau_{xy} v - \tau_{yz} w + q_y + \\ \Sigma_k(\rho_k h_k v diff_k) \\ \rho kv - \frac{\mu_t}{\sigma_k}\frac{\partial K}{\partial y} \\ \rho \epsilon v - \frac{\mu_t}{\sigma_\epsilon}\frac{\partial \epsilon}{\partial y} \\ \rho_{H2}(v + vdiff_{H2}) \\ \rho_{O2}(v + vdiff_{O2}) \\ \rho_{H20}(v + vdiff_{H20}) \\ \rho_{OH}(v + vdiff_{OH}) \\ \rho_H(v + vdiff_H) \\ \rho_O(v + vdiff_O) \\ \rho_{N2}(v + vdiff_{N2}) \\ \rho_{CO2}(v + vdiff_{CO2}) \end{pmatrix} \tag{5}$$

$$\mathbf{H} = \begin{pmatrix} \rho w \\ \rho wu - \tau_{xz} \\ \rho wv - \tau_{yz} \\ \rho w^2 + p - \tau_{zz} \\ w(p + e - \tau_{zz}) - \tau_{xz}v - \tau_{yz}w + q_z + \\ \Sigma_k(\rho_k h_k wdiff_k) \\ \rho kw - \frac{\mu_t}{\sigma_k}\frac{\partial K}{\partial z} \\ \rho \epsilon w - \frac{\mu_t}{\sigma_\epsilon}\frac{\partial \epsilon}{\partial z} \\ \rho_{H2}(w + wdiff_{H2}) \\ \rho_{O2}(w + wdiff_{O2}) \\ \rho_{H20}(w + wdiff_{H20}) \\ \rho_{OH}(w + wdiff_{OH}) \\ \rho_H(w + wdiff_H) \\ \rho_O(w + wdiff_O) \\ \rho_{N2}(w + wdiff_{N2}) \\ \rho_{CO2}(w + wdiff_{CO2}) \end{pmatrix} \tag{6}$$

$$\mu_t = \frac{C_\mu \rho k^2}{\epsilon} \tag{7}$$

where ρ is the gas density, and p the pressure of the mixture. The velocity components u,v and w are in the direction x, y and z respectively, e is the total internal energy of the mixture, k is the thermal conductivity of the mixture and T is the temperature and τ_{ij} is the viscous stress tensor.

The turbulence is modelled by means of K-ϵ model and μ_t is the turbulent viscosity. K is the kinetic energy of turbulence, ϵ is the dissipation rate and $C\mu$ is a constant = 0.09. The turbulent Prandtl number is taken as 0.92 and $udif f_i$ is the diffusion velocity of species i in x direction and is evaluated by assuming unity Lewis number.

3.2. Solver

The Navier-Stokes equation in the conservative form with species conservation equation is solved using standard finite volume method on an adaptive Cartesian Mesh. The interface fluxes are computed using an upwind scheme of the type AUSM. To ensure second order accuracy, linear reconstruction of primitive variables is done from the cell centre to the cell interface with a min-mod limiter. In the regions of strong gradients, the scheme becomes first order. The viscous fluxes are obtained by standard central differencing. The solution marches in time for each cell based on its local time step. Since the species conservation equations are very stiff due to highly non-linear production terms, a point implicit scheme is adopted for the conservation equations alone to accelerate the flow solution. The species production rates are estimated from 7 reaction model of ONERA ([6]) and given in Table 1.

Table 1. H2-Air Reaction model

Reaction	A,mol-cm-s	b	C,K
$H_2+O_2 \rightarrow 2OH$	$1.700X10^{13}$	0.0	24044
$2OH \rightarrow H_2+O_2$	$4.032X10^{10}$	0.317	14554
$H+O_2 \rightarrow OH+O$	$1.987X10^{14}$	0.0	8456
$OH+O \rightarrow H+O_2$	$8.930X10^{11}$	0.338	-118
$H_2+OH \rightarrow H_2O+H$	$1.024X10^{8}$	1.6	1660
$H_2O+H \rightarrow H_2+OH$	$7.964X10^{8}$	1.528	9300
$H_2+O \rightarrow OH+H$	$5.119X10^{4}$	2.67	3163
$OH+H \rightarrow H_2+O$	$2.701X10^{4}$	2.649	2240
$2OH \rightarrow H_2O+O$	$1.506X10^{9}$	1.14	50
$H_2O+O \rightarrow 2OH$	$2.220X10^{10}$	1.089	8613
$H+OH+M \rightarrow H_2O+M$	$2.212X10^{22}$	-2.0	0.0
$H_2O+M \rightarrow H+OH+M$	$8.936X10^{22}$	-1.835	59743
$2H+M \rightarrow H_2+M$	$9.791X10^{16}$	-0.6	0.0
$H_2+M \rightarrow 2H+M$	$5.086X10^{16}$	-0.362	52105

The first reaction mentioned in the table is a chain initiation reaction and the second and fourth reactions are chain branching reactions. The third reaction is a chain propagation reaction and the sixth reaction is a chain termination reaction. Formation of Hydroxyl radical(OH) is a very important step in the combustion of H_2 and O_2.

$H_2 + O_2 \rightarrow 2OH$ is the forward reaction and $2OH \rightarrow H_2 + O_2$ is the backward reaction. Forward and backward reaction rates are expressed by the formula

$\omega_f = k_f \Pi_s[As]^{\alpha s}$ and $\omega_b = kb\Pi_s[B_s]^{\beta s}$

where k_f and k_b are the forward and backward reaction rate constants and $[A_s]$ and $[B_s]$ are the mole concentrations of species on the left and right hand sides of the reaction formula, α_s and β_s are the species stoichometric coeffcients.

The reaction rate constant is determined by the Arrhenius formula:

$k=AT^b\exp(-C/T)$

where the parameters A,b and C are given in the table above for the forward and backward reactions. The concentration of the third body [M] is equal to the sum $\Sigma[A_s]K_{ef\,fs}$ where $K_{ef\,fs}$ is the efficiency of the species. The third body efficiency of H_2O was taken equal to 12 and the efficiency of H_2 equal to 2.5 and for the other species including N_2 and CO_2, equal to 1. It is necessary to consider CO_2 as separate species since specific heat of CO_2 is different from that of N_2 and will alter the temperature of gas mixture and thus the reaction rate. No coupling is assumed between the turbulence and chemical kinetics, which means the reaction rates are calculated for mean temperature and mean species concentrations. This assumption is debatable, as depending on the mixing time and chemical reaction time, the interaction could be important. However, the assumption of no turbulence chemistry interaction makes the combustion model much simpler.

PARAS-3D CFD code can handle complex geometries and has already been applied to a lot of practical problems. The modeling and the software have been validated with ground test results ([7], [8]). The test conditions to the scramjet combustor are Mach number 2.0, pressure 1.2bar and stagnation temperature 1600K. Fuel is injected through struts with 16° angle. The code is able to predict the trend as well as magnitude within 10% accuracy for pressure (fuel Equivalence Ratio ER 0.8).

4. COMBUSTOR GEOMETRY & FLOW DETAILS

Combustor geometry considered for the study is shown in Figure 2. It has rectangular cross section with constant area region followed by divergent area region. Length is 14.3H and width is 4H (H is the height of the combustion chamber at entry). Fuel is injected through three equi-spaced strut configuration similar to that used in [9]. Struts have leading edge in the front and ramps in the rear from the base of which fuel is injected through discrete circular holes in the near axial direction. Holes are provided at the strut base for pilot flame jets to help ignition, which are not considered in this study.

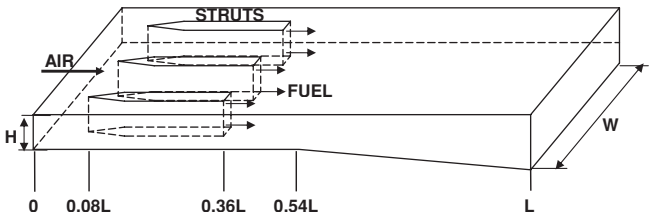

Figure 2. Combustor geometry

Hydrogen gas is injected at sonic speed and at stagnation temperature of 300K. Pressure of injection is varied to suit the fuel equivalence ratio simulated. Air enters the combustor at Mach 2.7 and at a stagnation temperature of 1920K (corresponding to a flight Mach number of about 6.5). Different pressure of combustor entry is considered for the study and are mentioned in each case.

In all cases the entry profile of all properties are uniform except for the cases where the effect of non-uniformity is studied. The composition of air considered for the study is 78% N_2 and 22% O_2 by mass fraction in all cases except for the case where effect of vitiation is studied.

5. COMPUTATIONAL DETAILS

Computational domain used for the studies is shown in Figure 3. Considering the symmetry of the combustor configuration, computations are carried out for half geometry. The following boundary conditions are employed. Boundary condition at Xmin-Supersonic Inflow, at Xmax-Supersonic outflow, at Ymin, Ymax and Zmin-Wall and at Zmax -Symmetry . Wall boundary conditions are handled by means of a modified wall function ([10]).

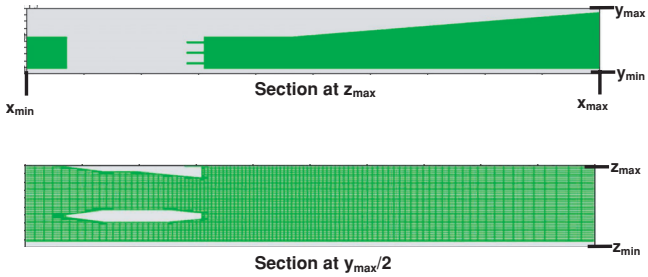

Figure 3. Computational grids and domain

Initial grid size of 100X100X50 is used for generating the combustor geometry and after refinement the total number of grids is 15lakhs. Fuel is injected through multiple circular holes distributed on the base of the strut/ramp. Very fine mesh is used near the hole and "oct-tree-division" based on body curvature (up to level 4) is adopted to capture the hole as close to circular geometry. (Please note here that the effect of minor variation of the geometry from being a perfect circle on the mass flow rate of fuel injected is taken care of by tuning the fuel injection pressure). To arrive at grid independence, computations are carried out with initial grid of 2lakh, 5lakh and 12lakh cells ([7]). Less than 5% difference is observed in pressure distribution between last two cases (5lakh cells & 12lakh cells). All simulations are carried out with 5lakh initial cells. Iteration convergence for pressure, H2 consumption, H_2O & OH formation and total temperature rise are monitored. Convergence plot for H_2O formation with entry pressure 0.35bar & ER 0.65 is shown in Figure 4. Also, convergence plot for area averaged pressure ratio with entry pressure 0.35bar & ER 0.65 is shown in Figure 5. Variation in properties between 50000 & 80000 iteration is very small (less than 2%). Hence all studies are carried out up to 50000 iterations. Adequacy of 50000 iterations at lower pressure & lower ER is also checked and Figure 6 shows the convergence plot for H_2O formation for entry pressure 0.17bar & at ER 0.42.

6. RESULTS & DISCUSSION

All computations are carried out for combustor entry Mach number of 2.7 and stagnation temperature of 1920K as already mentioned and for two representative fuel equivalence ratios (ER) of 0.42 & 0.65. The study is carried out under three categories i) effect of pressure, ii) effect of vitiation and iii) effect of entry flow profile. Results in this section are given as mass averaged across combustion chamber cross section for all parameters except for pressure which is area averaged and are plotted with respect to length of combustion chamber. However, for a typical case, the progress of reaction is provided. Figure 7 depicts H_2O mass fraction at different cross sections along the combustion chamber.

6.1. Effect of pressure

Computations are initially carried out for a representative nominal combustor entry pressure of 0.35bar (for a typical flight Mach number of 6.5, dynamic pressure 60kPa and pressure recovery of about 15%) and for higher pressure 0.52bar (i.e., 0.35X1.5) and lower pressure 0.23bar (i.e., 0.35/1.5). H_2 consumption for the three cases at ER 0.42 & 0.65 is shown in Figure 8. Sharp increase in H_2 consumption is noticed just downstream of struts and more than 90% of H_2 is consumed by end of the combustor. However one case, showed a different pattern in the H_2 consumption. It is lacking just downstream of strut but picks up later and goes to about 93%. This prompted us to carry out computations for pressure lower than 0.23bar and were carried out at entry pressure of 0.35/2± 0.03bar (i.e., 0.20bar, 0.17bar & 0.14bar). Whatever is observed at ER 0.42 & combustor entry pressure 0.23bar is seen at ER 0.65 & combustor entry pressure 0.17bar (Figure 9). Again in this cases, H_2 consumption at end of the combustor goes to about 90%.

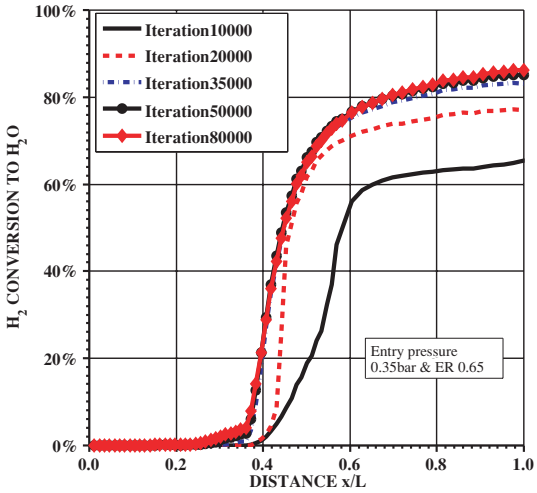

Figure 4. Iteration convergence plot for H_2O formation(entry pressure 0.35bar & ER 0.65)

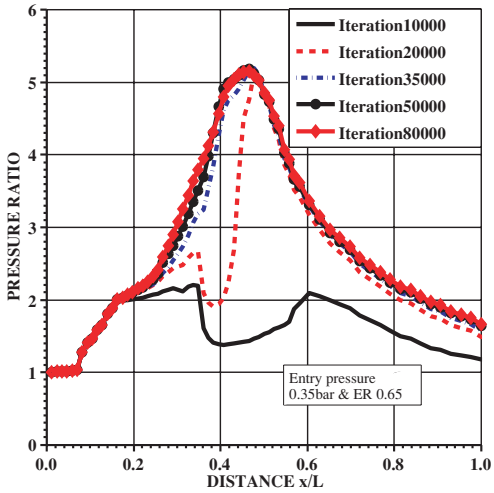

Figure 5. Iteration convergence plot for pressure distribution (entry pressure 0.35bar & ER 0.65)

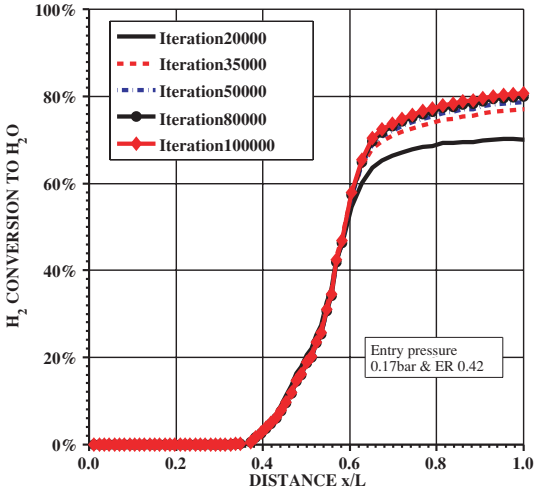

Figure 6. Iteration convergence plot for H_2O formation(entry pressure 0.17bar & ER 0.42)

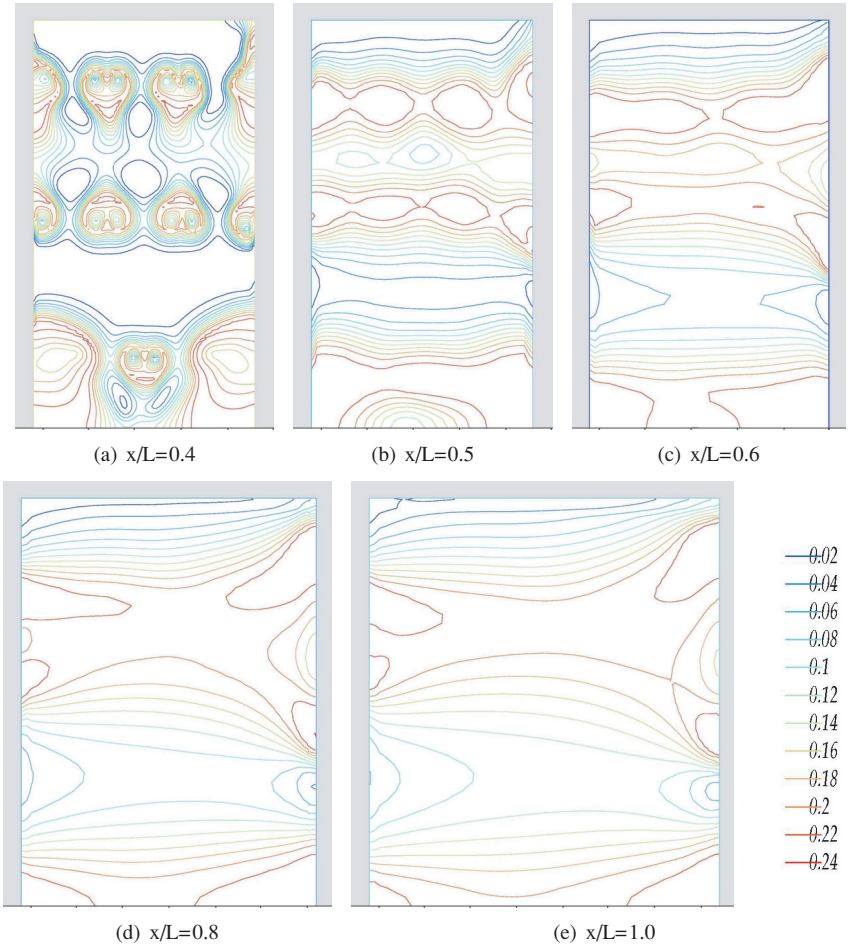

Figure 7. H_2O mass fraction at different cross sections; entry pressure 0.35bar & ER0.65. (Symmetry plane at bottom & divergent side at right)

Total temperature rise for various pressure studied are shown in Figure 10 and Figure 11 for ER 0.65 & 0.42 respectively. Two major observations are made (i) at lower pressure there is a initial fall in the total temperature downstream of strut and (ii) the final temperature at exit of combustion chamber is lower for low entry pressures though H_2 consumption is roughly same for all cases at exit of combustion chamber.

Normally higher rate of H_2 consumption takes place downstream of strut with high heat release. Without heat release the resultant temperature could have fallen due to the low temperature of hydrogen gases and due to its high specific heat (though the flow ratio is small). This explains the initial fall in the total temperature for low pressure cases. Regarding the low temperature at exit of combustor even when H_2 consumption is nearly same, conversion of H_2 to its reaction products is studied in detail.

In Figure 12 & Figure 13, H_2 conversion to H_2O is shown for ER 0.65 & 0.42 respectively. H_2 conversion to H_2O is ratio of actual H_2O formation to complete conversion of H_2 to H_2O (i.e., total H_2 flow rate*18.016/2.016). H_2 conversion to OH is ratio of actual OH formation to complete conversion of H_2 to OH (i.e., total H_2 flow rate*17.008/1.008). H_2 conversion to H is ratio between H flow rate and complete H_2 conversion to H (i.e., total H2 flow rate). It is clear that at lower pressure though H_2 is getting consumed it is not always getting converted into H_2O but OH & H is being formed at higher levels (Figure 14 & Figure 15). Similar thing is observed in ER 0.42 and is shown in Figure 16 & Figure 17. But deviation occurs at higher entry pressure than in the case of ER 0.65. This is explainable by the fact that low ER leads to lower levels of pressure rise in combustion zone there by they behave like low pressure cases for higher equivalence ratios. In the cases studied, pressure limit is about 0.17bar for fuel equivalence ratio 0.65 and about 0.23bar for fuel equivalence ratio 0.42.

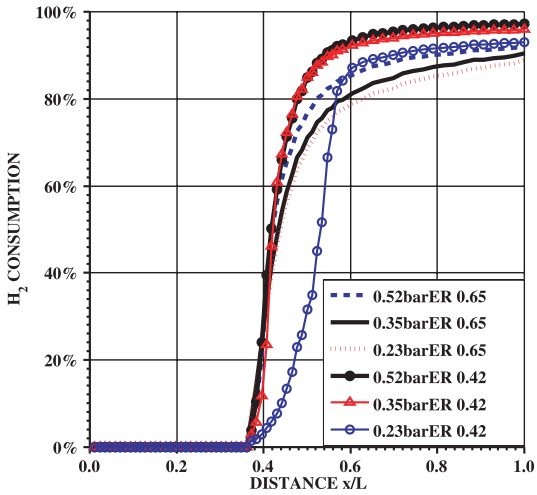

Figure 8. H_2 consumption for different entry pressures (at ER 0.65 & ER 0.42)

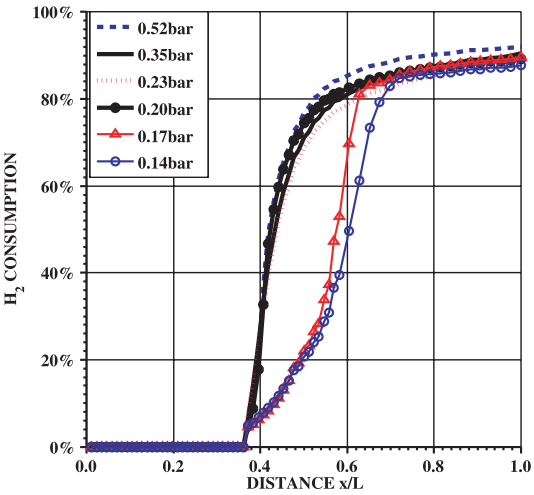

Figure 9. H_2 consumption for different entry pressures (at ER 0.65)

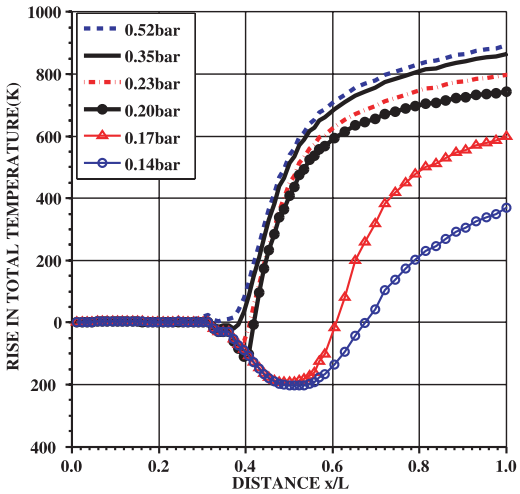

Figure 10. Rise in total temperature for different entry pressures (at ER 0.65)

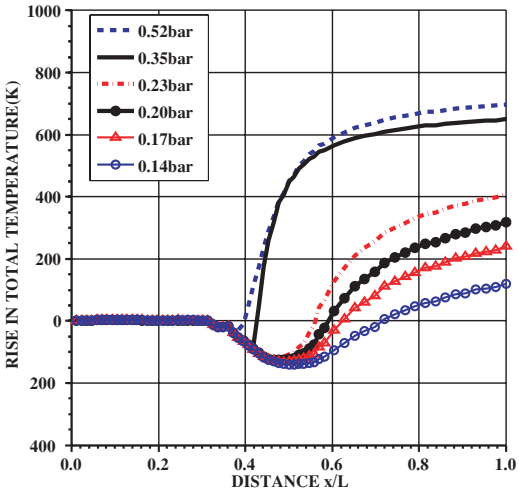

Figure 11. Rise in total temperature for different entry pressures (at ER 0.42)

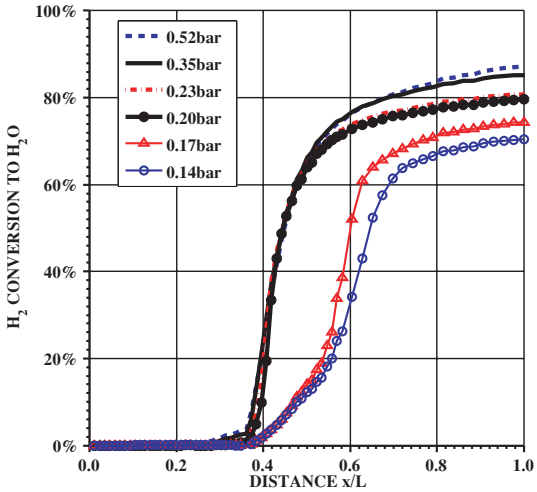

Figure 12. H_2 conversion to H_2O for different entry pressures (at ER 0.65)

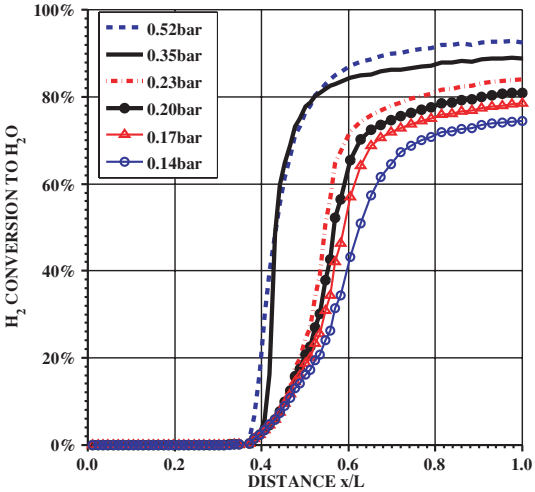

Figure 13. H_2 conversion to H_2O for different entry pressures (at ER 0.42)

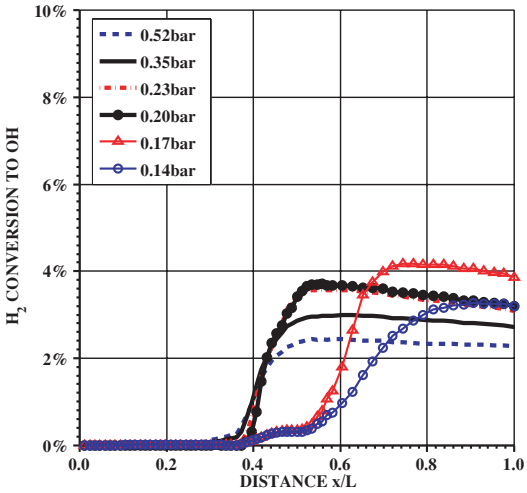

Figure 14. H_2 conversion to OH for different entry pressures (at ER 0.65)

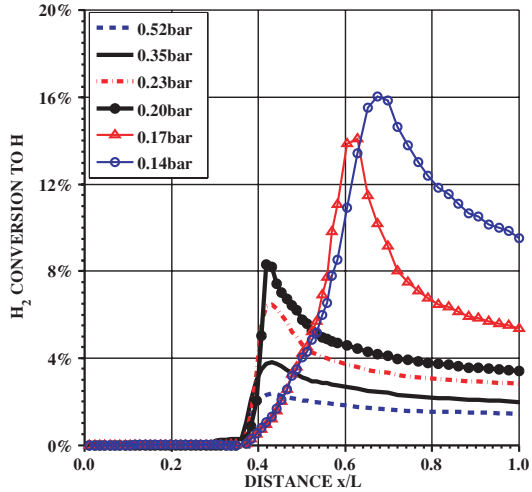

Figure 15. H_2 conversion to H for different entry pressures (at ER 0.65)

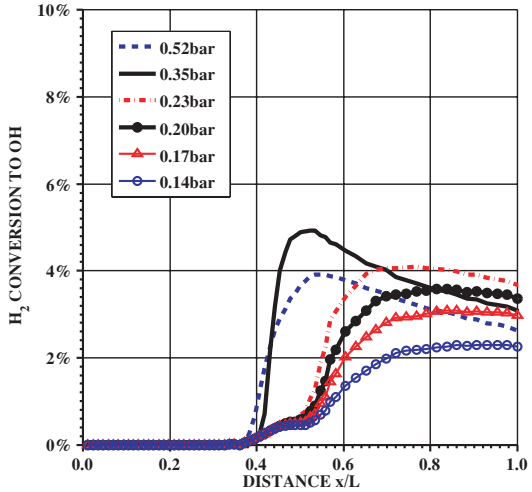

Figure 16. H_2 conversion to OH for different entry pressures (at ER 0.42)

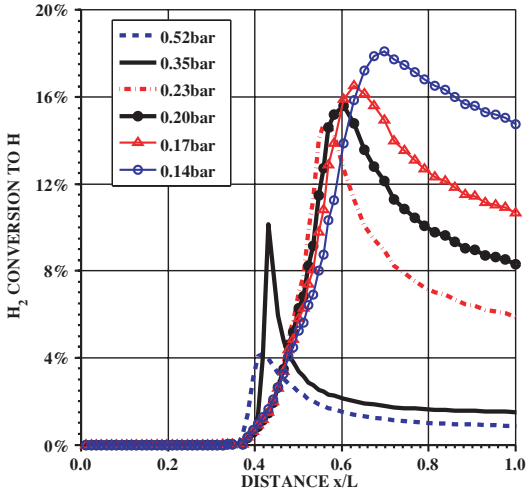

Figure 17. H_2 conversion to H for different entry pressures (at ER 0.42)

6.2. Effect of vitiation

Computations are carried out to bring out the vitiation effect for a chosen combustor entry pressure of 0.52bar. For a typical vitiated air heater, where a hydrocarbon fuel like ethanol is used, combustor entry medium will have H_2O & CO_2 replacing some portion of N_2. Oxygen is replenished and brought to mass fraction level of clean air. As a representative composition, O_2 22%, $N2$ 59%, H_2O 7.5% and CO_2 11.5% by mass fraction (molecular weight about 30) is chosen for the vitiated medium. As it is not possible to simulate all flow parameters at combustor entry as in the case of clean air, in this study, the parameters that have been matched at the combustor entry are oxygen mass fraction (22%), pressure (0.52bar), Mach number (2.7) and total temperature (1920K). (In this process, mass flow rate is about 5% less compared to that of clean air due to slight variation in specific heat ratio and molecular weight).

In the case of vitiated medium, rise in total temperature is about 8% less than that in the case of clean air at ER 0.42 and is shown in Figure 18. Whereas at higher ER (0.65) the reduction of total temperature rise is more (about 15%). This results in variation in the pressure distribution in the combustion chamber and is shown in Figure 19. Pressure rise in the combustion chamber is about 10% lower in the case of vitiated medium at ER0.42 and is about 19% lower at ER0.65. The presence of CO_2 and the excess H_2O present will tend to absorb more heat resulting in lower total temperature and there by lower pressures in the combustion chamber.

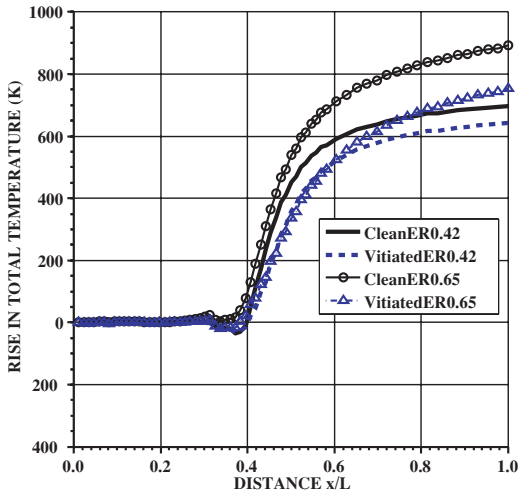

Figure 18. Total temperature rise for clean air & vitiated air (at ER 0.42 & ER 0.65)

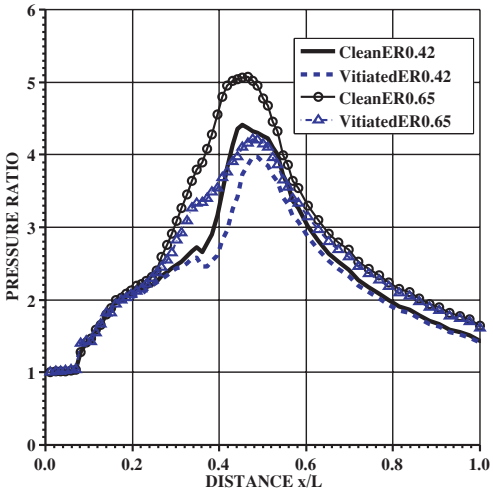

Figure 19. Pressure distribution for clean air & vitiated air (at ER 0.42 & ER 0.65)

6.3. Effect of entry flow profile

Computations are carried out for full engine consisting of hypersonic air intake, combustor & nozzle to compare the results with isolated combustor geometry simulation. Engine is considered to be mounted on a cone-cylinder fore body with boundary layer splitter-diverter between cylinder and air intake. In order to simulate a real flow properties at the combustion chamber entry, typical air intake is considered and it consists of two ramps followed by expansion corner on the body side and drooped cowl on the opposite side. Engine with fore-body is simulated at free-stream Mach number of 6.5 & dynamic pressure of 60kPa and it gives combustor entry pressure of 0.52bar, Mach number 2.7 & total temperature 1920K. Mass averaged Mach number & area averaged pressure closely match for both cases and there is a small change in mass averaged total temperature of the order of 50K observed. Combustor entry profile for pressure, Mach number, total temperature & velocity are shown in Figure 20. *"Degree of non-uniformity"* is calculated using the expression $\sqrt{\Sigma(X/\overline{X}-1)^2\Delta\dot{m}/\dot{m}}$ (where X is the flow parameter, $\overline{X}$ is the mass averaged flow parameter and $\dot{m}$ is the mass flow rate) and $\sqrt{\Sigma(X/\overline{X}-1)^2\Delta A/A}$ (where X is the flow parameter, $\overline{X}$ is the area averaged flow parameter and A is the combustion chamber cross section area). *"Degree of non-uniformity"* (at combustor entry) of pressure is about 25%, Mach number & velocity is about 10% and total temperature is about 5%.

In the case of full engine simulation, non-uniform profile at combustor entry leads to lower rise of total temperature for both equivalence ratios. Form Figure 21, it is observed that, total temperature rise for the case of non-uniform profile is about 10% lower for ER 0.42 and about 17% lower for 0.65. Reason for the reduction in total temperature is due to reduced conversion of H_2 to H_2O in the case of non-uniform profile (Figure 22). This is explained by the lack of mixing between H_2 and air which is reflected by the *"degree of non-uniformity"* of H_2O at the exit of combustor. This parameter is about 35% for uniform combustor entry conditions, which is about 55% for non-uniform entry conditions at ER 0.65.

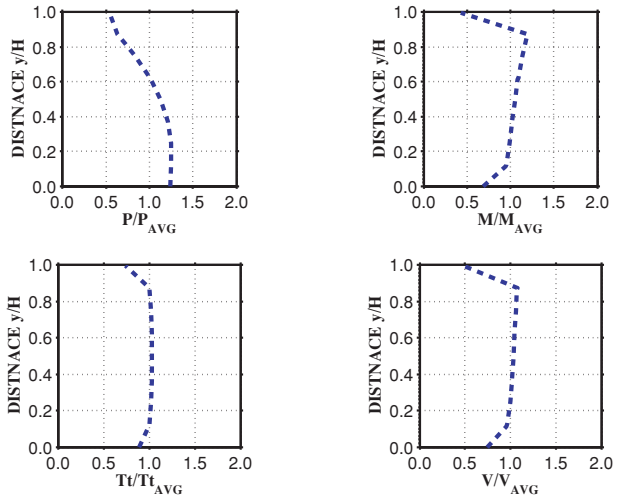

Figure 20. Combustor entry profile at symmetry plane for full engine simulation (P-static pressure, M-Mach number, Tt-Total temperature & V-Total velocity

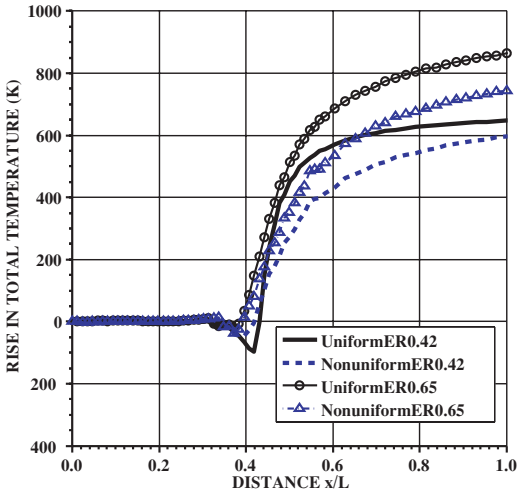

Figure 21. Total temperature rise for uniform & non-uniform combustor entry floe profie (at ER 0.42 & ER 0.65)

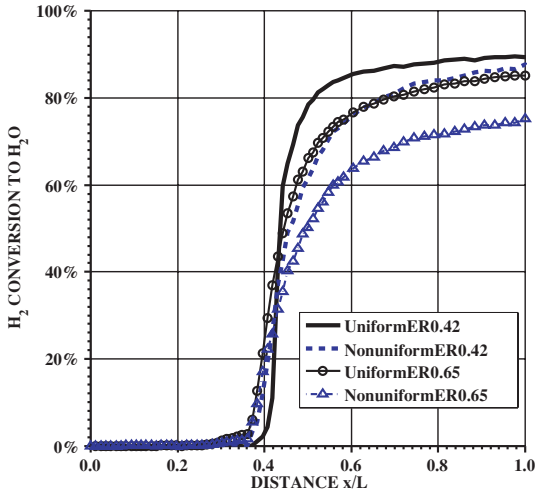

Figure 22. H_2 consumption for uniform & non-uniform combustor entry floe profile (at ER 0.42 & ER 0.65)

7. CONCLUDING REMARK

CFD computations are carried out for evaluating the performance of a scramjet combustor under connected pipe test conditions for two equivalence ratios. Computations are carried out under three categories i) effect of pressure, ii) effect of vitiation and iii) effect of entry flow profile. Combustor entry pressure is having substantial influence on scramjet combustor performance at pressures lower than certain limit. This pressure limit is also found to vary with equivalence ratio. In the cases studied, this pressure limit is about 0.17bar for fuel equivalence ratio 0.65 and about 0.23bar for fuel equivalence ratio 0.42. At lower pressures of entry, the progress of combustion is low, causing a drop of upto 500K in the combustor exit total temperature, for a reduction of combustor entry pressure by half.

In the case of vitiated medium studied, the total temperature rise is 10 to 15% less compared to clean air. In the combustion chamber, pressure rise is also less by about 10 to 20% for the vitiated medium. Non-uniform flow profile at combustor entry reduces the scramjet combustor performance. It is found that a degree of non-uniformity (as defined) of about 20% leads to about 10 to 20% reduction in combustor exit total temperature. These results are useful in extrapolating the connected pipe combustor ground test results to flight environment.

ACKNOWLEDGEMENT

Authors thank Mr.Amit Sachdeva, Engineer, ADTG/VSSC and Mr. C. Lavaraj, Engineer, ABPP/VSSC for their contribution towards combustor geometry generation and data processing.

Mr. S. Ramakrishnan, Director, Projects, VSSC and Dr. K. Radhakrishnan, Director, VSSC are gratefully acknowledged for the encouragement provided and the permission to publish this work.

REFERENCES

[1] Pellett, G.L., Claudio Bruno and Chinitz, W., "Review of air vitiation effects on scramjet ignition and flameholding combustion processes", 38th Joint Propulsion Conference and Exhibit, July 2002, AIAA 2002-3880.

[2] Edelman, R.B., and Spadanccin, L.J., "Theoretical Effects of Vitiated Air Contamination on Ground Testing of Hypersonic Air breathing Engines", Journal of spacecraft, Vol.6, No.12, 1969.

[3] Mitani, T., et al., "Scramjet engine testing in Mach 6 vitiated air", 7th International space planes and hypersonic systems and technologies conference, 1996, AIAA 96-4555.

[4] Goyne, C.P., Krauss, R.H., McDaniel, J.C. and Whitehurst, W.B., "Test Gas Vitiation Effects in a Dual-mode Scramjet Combustor," Journal of Propulsion and Power, Vol. 23, No. 3, 2007.

[5] Ashok, V., Pradeep Kumar, Thomas C. Babu and Devasia, KJ., "Users Manual for PARAS-3D", VSSC/ARD/TR-033/2000.

[6] Dmitry Davidenko, Iskender Gokalp, Emmanuel Dufour and Philippe Magre, "Numerical simulation of hydrogen supersonic combustion and validation of computational approach", 12*th* AIAA International Space Planes and Hypersonic Systems and Technologies, December 2003, AIAA 2003-7033.

[7] Ashok, V., "Numerical computation of flow with Hydrogen-Air combustion in a scramjet combustor", VSSC/ARD/TR/097/2006, September 2006.

[8] Ashok, V. and Dipankar Das, "End to end simulation of a typical scramjet flight technology demonstrator", VSSC/ADTG/TR/01/2007, November 2007.

[9] Scherrer, D., Dessornes, O., Montmayeur, N. and Ferrandon, O., "Injection studies in the French hypersonic technology program", 6th international aerospace planes and hypersonic technologies conference, April 1995, AIAA 95-6096.

[10] Hagmann, C., Schley, CA., Odinstov, E. and Sobatchkine, A., "Nozzle flow field analysis with particular regard to 3D-plug cluster configurations"', Joint propulsion conference & Exhibit, July 1996, AIAA-96-2954.